Comparison of the Characteristics of Cost-Oriented Designed High-Speed Low-Power Interior PMSM

Aryanti Kusuma Putri, Marco Hombitzer, David Franck, and Kay Hameyer, *Senior Member, IEEE*

***Abstract*—In this paper, the characteristics of interior permanent magnet synchronous machine (IPMSM) with concentrated windings are evaluated for three different rotor geometries. The reference machine is a fractional horsepower IPMSM with single-layer magnets (1-layered IPMSM). The maximum output power of the machine is 820 W. Based on the electrical properties and machine cost of the reference machine, IPMSM with two different rotor geometries are designed. The first one is an IPMSM with v-shaped magnets and the second one is an IPMSM with double-layer magnets topology (2-layered IPMSM). The machines are compared in two operating points: one in the base speed area and one in the field weakening range. The focus of the machine comparison is the parasitic effects due to the nonsinusoidal rotor field, e.g., back-EMF harmonics, torque harmonics, radial force densities, and iron losses.**

***Index Terms*—Air gap flux densities, low-cost machines, low-power drives, permanent magnet synchronous machines (PMSM), radial force densities, rotor pole shaping, torque harmonics.**

I. Introduction

THE PERMANENT magnet synchronous machines (PMSM) exhibit high power and torque density, when compared to other types of electrical machines. For this reason, PMSM are widely used in applications that have low-space and light-weight requirements. The torque of a PMSM can be decomposed in two components: the synchronous torque and the reluctance torque. The synchronous torque is generated by the interaction of stator and rotor fields. The reluctance torque is caused by the difference of the magnetic reluctance in direct and quadrature axes. Due to the homogeneous reluctance on both axes, a surface-mounted synchronous machine (SPMSM) possesses only a synchronous torque. The interior PMSM (IPMSM) exhibit a lower synchronous torque when compared to SPMSM. This can be compensated with the reluctance torque of the machine. To achieve higher power densities, the use of high-speed machines is increased in the recent years. Due to the good flux weakening capability of IPMSM, this type of machine is more attractive for applications with a wide constant-power range when compared to SPMSM [1], [2].

TABLE I
Geometrical and Electrical Requirements of the IPMSM

Stator outer radius $r_{\text{stator},o}$	60 mm
Minimum air gap length δ	0.7 mm
Axial length l_{Fe}	30 mm
Number of poles/slots $2p/N$	6/9
Magnet type	NdFeB
Minimum magnet height	2 mm
Winding type	Single-tooth winding
Maximum input voltage U_{line}	190 V
Maximum phase current I_{eff}	7.1 A

The objective of this paper is to compare different types of IPMSM regarding its characteristics in different working areas: base speed area ($n_1 = 610\,\text{min}^{-1}$ and $M_1 = 1.31\,\text{N}\cdot\text{m}$) and field weakening range ($n_2 = 19\,520\,\text{min}^{-1}$ and $M_2 = 0.26\,\text{N}\cdot\text{m}$). The main issue of the machine design is the speed difference of both operating points, whose ratio is $n_1 : n_2 = 1 : 32$. Furthermore, the available construction space of the machine is strongly limited. In Table I, the geometrical and electrical requirements of the machine are listed.

Three different rotor geometries are studied and examined concerning the parasitic effects in the chosen working points, e.g., back-EMF harmonics, torque harmonics, radial force densities, and iron losses. The basic geometries of the rotors are shown in Fig. 1. The basic geometry represents the rotor geometry without modification on its surface (round rotor). In Fig. 1(a), the basic geometry of the reference machine, IPMSM with single-layer magnets (1-layered IPMSM), is shown. To reduce the torque ripple and the back-EMF harmonics, the surface of the rotor is modified by the methods introduced in [3] and [4]. In Fig. 1(b) and (c), the basic geometries of the alternative machines are drawn. These are IPMSM with v-shaped magnets (VPMSM) and IPMSM with double-layer magnets (2-layered IPMSM), which exhibit high ratio of reluctance to overall torque. Through the utilization of the reluctance torque, alternative machines with lower cost and equivalent qualities to the reference machine, such as the torque ripple and the acoustic radiation, are designed. The characteristics of the final machines will be evaluated and compared with the reference machine.

II. Simulation

By a finite-element model, the rotor angle dependent back EMF, torque and torque harmonics, radial force densities, and iron losses are simulated.

Manuscript received October 17, 2016; revised March 3, 2017; accepted June 22, 2017. Date of publication June 27, 2017; date of current version November 20, 2017. Paper 2016-EMC-1033.R1, presented at the 2016 22nd International Conference on Electrical Machines, Lausanne, Switzerland, Sep. 4–7, and approved for publication in the IEEE Transactions on Industry Applications, by the Electric Machines Committee of the IEEE Industry Applications Society. *(Corresponding author: Aryanti Kusuma Putri.)*

The authors are with the Institute of Electrical Machines, RWTH Aachen University, Aachen 52062, Germany (e-mail: aryanti.putri@iem.rwth-aachen.de; marco.hombitzer@iem.rwth-aachen.de; david.franck@iem.rwth-aachen.de; kay.hameyer@iem.rwth-aachen.de).

Color versions of one or more of the figures in this paper are available online at http://ieeexplore.ieee.org.

Digital Object Identifier 10.1109/TIA.2017.2720663

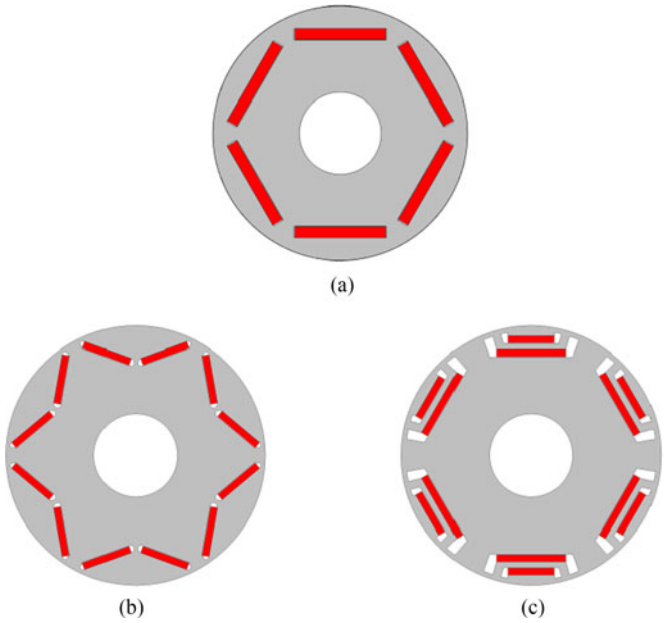

Fig. 1. Basic geometry of the examined rotors. (a) 1-layered IPMSM, (b) VPMSM, and (c) 2-layered IPMSM.

The back EMF of each phase is determined through the differentiation of the phase magnetic flux for every rotor angle, which is calculated through the surface integration of the flux density B for every element of each winding. In the next step, the resistance of each winding R_1 is considered by a multiplication with the phase current i_1. The line-to-line voltage u_{line} is calculated by subtraction of two phases. It can be described with the following equations:

$$u_{\text{phase},1}(t) = -\frac{d}{dt}\iint B(t)\,dA + i_1(t)R_1$$
$$u_{\text{line},12}(t) = u_{\text{phase},1}(t) - u_{\text{phase},2}(t). \tag{1}$$

The torque and the torque harmonics are calculated by the methods introduced in [5], which is based on the eggshell method [6]. The sum of the forces F_k on every node k (nodal force) multiplied by its distance to the origin of the rotor r_k represents the torque T at one point in time

$$T = \Sigma\, r_k \times F_k. \tag{2}$$

Employing (2) for multiple time steps for one rotation of the rotor, the mean torque and torque harmonics can be determined.

The radial force densities acting on the stator are evaluated through the decomposition of the nodal forces in the tangential and radial components, which are normalized to the length of the machine. The radial force densities can be decomposed by the two-dimensional Fourier transformation in time and spatial orders. The sensitive hearing range of humans lies between 2 and 5 kHz [7]. To estimate the acoustic radiation of the machines, the occurred low spatial orders within this frequency range with a deviation of 1 kHz are compared.

TABLE II
a-PARAMETERS FOR IRON LOSS CALCULATION

a_1	$88.74 \cdot 10^{-3}$
a_2	$73.76 \cdot 10^{-6}$
a_3	$284.40 \cdot 10^{-3}$
a_4	3
a_5	0

The iron losses are calculated by the IEM-formula for electrical machines, which is described in [8] and [9]:

$$P_{v,Fe} = a_1\, B^2\, f_{el.} + a_2\, B^2\, f_{el.}^2\,(1 + a_3\, B^{a_4}) + a_5\, B^{1.5}\, f_{el.}^{1.5}. \tag{3}$$

where $f_{el.}$ and a_1 to a_5 are electrical frequency and the iron loss parameters, respectively. The parameters are listed in Table II. These are derived from the manufacturer data and fitted according to the measurements in two working points of the reference machine. The iron losses are calculated for each element in every time step and the harmonics of flux density B are taken into account.

III. DESIGN

In this section, the machine requirements and the design methods of the alternative machines are described. The stator geometry parameters, such as the height of the yoke and the width of the stator teeth, are kept constant. Hence, the acoustic radiation level can be estimated by the calculation of the radial force densities. The combination of the rotor poles and stator slots is not changed, so that the dominant temporal and spatial orders of the force excitations are preserved. To achieve lower cost, the magnet volume of the alternative machines shall not exceed the magnet volume of the reference machine.

A. Machine Requirements

The reference machine has two operating points: base speed area with speed $n_1 = 610\,\text{min}^{-1}$ and torque $M_1 = 1.31\,\text{N}\cdot\text{m}$ (OP 1) and field weakening range with speed $n_2 = 19520\,\text{min}^{-1}$ and torque $M_2 = 0.26\,\text{N}\cdot\text{m}$ (OP 2). The electrical operating points are defined by the control of maximum torque per ampere and maximum torque per voltage, which are described in [10]. In Table III, the simulation results of the relevant operating points are listed. These serve as the design orientation of the alternative machines. The minimum efficiency in OP 1 and OP 2 are 62% and 74% at the winding temperature of 70 °C, respectively. Furthermore, the required maximum output power $P_{\max}$ is 820 W and the minimum output power between the speed $n = 5000 - 20\,000\,\text{min}^{-1}$ is $P_{\min} = 700\,\text{W}$. The rotor surface velocity at $n = 20\,000\,\text{min}^{-1}$ is 60 m/s. In Table IV, the frequencies of the dominant temporal orders dependent on the operating points are listed. It can be concluded that only the force excitations in OP 2 are relevant for the acoustic radiation.

From Table III, it can be concluded that the copper losses are dominant in both operating points. To prevent the increase in

TABLE III
OPERATING POINTS OF THE REFERENCE MACHINE

	OP 1	OP 2
Speed (r/min)	610	19520
Torque (N · m)	1.31	0.26
Output power (W)	83.68	531.47
Copper losses (W)	38.68	60.62
Iron losses (W)	3.14	42.60
Efficiency (%)	66.14	78.90
Torque ripple (N · m)	0.03	0.01
Radial Force Density Orders (Temporal, Spatial) (kN/m^2)		
(6, −3)	15.26	5.35
(6, 6)	35.36	8.59
(12, −6)	1.81	1.12
(12, 3)	2.89	1.56
(18, 0)	0.49	0.16
Magnet volume (mm^3)	8820	

TABLE IV
FREQUENCIES OF THE RADIAL FORCE DENSITIES

	Frequency (Hz)	
Temporal Order	OP 1	OP 2
6	61	1952
12	122	3904
18	183	5856

these losses, the minimum amplitude of the flux density fundamental harmonic of the alternative machines is set to the amplitude of the flux density fundamental harmonic of the reference machine, which is 0.6 T.

One of the main causes of the parasitic effects in electrical machines, such as torque ripple and acoustic radiation, is the flux density harmonics of the rotor. These effects can be reduced through minimizing the total harmonic distortion (THD) of the rotor flux density. The THD is calculated as follows:

$$\mathrm{THD} = \sqrt{\frac{\sum_{\mu>1} {B_{\mathrm{rad}}^{\mu}}^2}{\sum_{\mu} {B_{\mathrm{rad}}^{\mu}}^2}}. \tag{4}$$

To ensure the mechanical stability, the rotors are designed to have the maximum stress of 350 MPa at $n = 30\,000\,\mathrm{min}^{-1}$, which is 1.5 times the maximum speed of the machines. Due to the manufacturing limitation, the minimum distance between the rotor bridges is set to 0.5 mm.

B. Design of the VPMSM

Due to the flux concentrating topology and high reluctance ratio L_q/L_d, VPMSM exhibits high synchronous and reluctance torque when compared to conventional 1-layered IPMSM with the same magnet mass [11]. The disadvantages of VPMSM compared to 1-layered IPMSM are, for example, the high cogging torque and torque ripple. To subdue this problem, the rotor alteration with the sinusoidal field pole method, described in [12], is applied on the rotor surface. Starting on the *d*-axis, the rotor's surface is formed, so that the induced rotor flux density follows a sinusoidal function. The rotor pole shaping is limited by the defined air gap ratio $\delta_\mathrm{q}/\delta_\mathrm{d}$. With this measure, the cogging torque and torque ripple of the VPMSM can be reduced [13]. The disadvantage of this surface alteration method is the reduction of the reluctance ratio L_q/L_d and thus the reluctance torque [14].

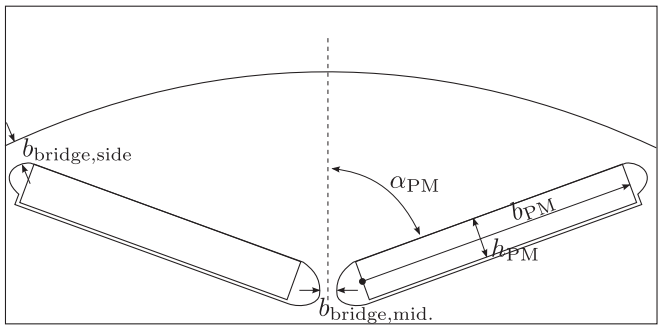

Fig. 2. Pole geometry of a VPMSM.

In Fig. 2, a pole of a VPMSM and its geometric parameters are shown. The pole pitch factor $\tau_\mathrm{PM}/\tau_\mathrm{p}$ is chosen to reach high effective torque and low torque ripple simultaneously. In case of a VPMSM, the optimal value of the pole pitch factor lies between 0.7 and 0.8 [15]. To minimize the leakage flux, the side bridge and the middle bridge between the poles ($b_{\mathrm{bridge,side}}$ and $b_{\mathrm{bridge,mid.}}$, respectively) have to be kept thin. The first design step is the variation of the magnet angle α_PM at a constant pole pitch factor. The magnet height is kept at its minimum value. The width of the permanent magnet increases with smaller magnet angle, which leads to a larger area of the magnet's surface in the magnetization direction and increase in the synchronous torque. Due to less amount of electrical steel, the inductance in the *d*-axis decreases with smaller magnet angle and, thus, the reluctance torque increases. As a conclusion, the effective torque of the machine increases with smaller magnet angle.

Through minimizing the used amount of magnet materials, the overall cost can be reduced. Hence, the permanent magnet width is reduced until the minimum amplitude of the rotor flux density fundamental harmonic in the air gap is reached. In Fig. 2, the reduction of the permanent magnet width is illustrated through the arrow with a dot at its starting point. The position of the starting point is kept constant, only the length of the arrow is reduced. The amount of the magnet material is decreased without changing the reluctance of the machine. The last design step of the VPMSM is the rotor surface modification according to Richter [12] to reduce the THD of the rotor flux density.

C. Design of the 2-Layered IPMSM

The 2-layered IPMSM possesses, in general, low synchronous torque when compared to 1-layered IPMSM. However, the saliency of a 2-layered IPMSM is superior to a 1-layered IPMSM. This compensates the disadvantage regarding the synchronous torque. It is illustrated in [16] that a 2-layered IPMSM can reach higher efficiency than 1-layered IPMSM without additional increase in magnet material. To maintain the reluctance

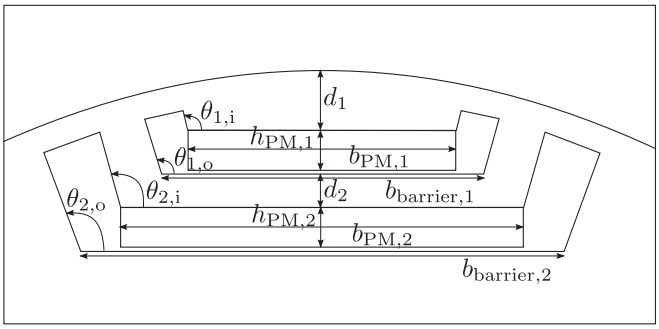

Fig. 3. Pole geometry of an IPMSM.

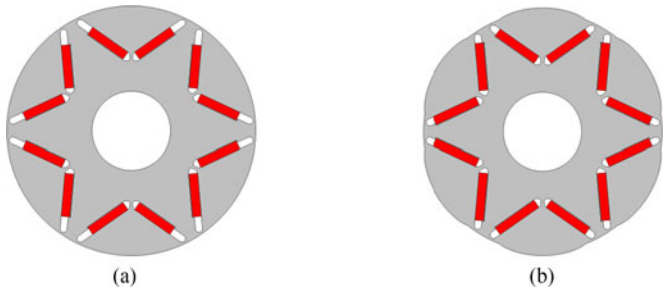

Fig. 4. Geometry of the designed VPMSM rotors. (a) VPMSM 1 and (b) VPMSM 2.

TABLE V
ROTOR PARAMETERS OF THE DESIGNED VPMSM

		VPMSM	
		Alt. 1	Alt. 2
Air gap ratio δ_q/δ_d	–	1	2.25
Pole pitch factor	–	0.77	
α_{PM}	°	55	
h_{PM}	mm	2	
b_{PM}	mm	10	11
$b_{\mathrm{bridge,mid}}$	mm	0.8	
$b_{\mathrm{bridge,side}}$	mm	0.5	

TABLE VI
VARIATION OF AIR GAP RATIO δ_q/δ_d

Air gap ratio δ_q/δ_d	Fundamental Harmonic B_1 (T)	THD (%)
1	0.68	27.11
1.5	0.65	13.34
1.75	0.66	8.5
2	0.66	5.22
2.25	0.66	3.62
2.5	0.66	3.16
3	0.66	3.14

torque, measures to reduce parasitic effects through the modification of the rotor's surface will not be taken. The measures to minimize the parasitic effects of a 2-layered IPMSM is studied in [17]. Through the variation of the flux barrier angles, the torque ripple and the radial force excitation of a 2-layered IPMSM can be minimized.

In Fig. 3, a pole of a 2-layered IPMSM and its geometry parameters are shown. Theoretically, a small distance of the permanent magnets to the air gap is advantageous. The amplitude of the rotor flux density increases with smaller distance to the air gap. However, this is only a minor effect when compared to the permanent magnet width. It is advantageous to have larger distances d_1 and d_2 than smaller permanent magnet widths. Moreover, the distance between the air gap and the first magnet d_1 is required, so that the flux barrier angles of the first permanent magnet can be variated without limitation. The barrier width b_{barrier} affects the form of the air gap flux density, particularly the first slope after the intersection of the poles. An approximation of a sinusoidal air gap flux density can be attained by the design of the barrier width. This effect can also be achieved through the variation of the flux barrier angles of the second permanent magnet.

The 2-layered IPMSM will be designed based on the sum of the magnet material of the VPMSM with rotor surface modification. The first step is to choose the ratio $b_{\mathrm{PM},1}/b_{\mathrm{PM},2}$. The height of both magnets is kept at its minimum value. The objective is to design a rotor that induces high air gap flux density with sufficiently low THD. The position of the magnets is changed dependent on the magnet width.

After choosing the suitable magnet ratio, the flux barrier angles of both permanent magnets are varied. The outer flux barrier of the second permanent magnet $\theta_{2,\mathrm{o}}$ correlates to the first slope after the pole intersection. This has to be designed as wide as possible, so that the rotor flux density at the pole intersection follows the sinusoidal function. The last design step of the IPMSM is the variation of the remaining flux barrier angles. The objective is to find a flux barrier combination, which generates a sufficient amplitude of the flux density fundamental harmonic and simultaneously low THD.

IV. SIMULATION RESULTS

In this section, the designed rotor for the alternative machines and the simulation results of the machine operating area are presented. First, the air gap flux densities of the rotors are analyzed. In the next step, machine parameters, back EMF, and cogging torque in the no-load operating point are evaluated. In base speed (OP 1) and field weakening area (OP 2), torque ripple, radial force excitation, and copper and iron losses are analyzed. In addition to [18], the analysis of the machine characteristics in the whole operating area is presented.

A. Designed Rotors

In Fig. 4, the geometry of the designed VPMSM rotors is shown. The geometry parameters are listed in Table V. The first rotor (VPMSM 1) is a rotor without the surface modification. The required magnet volume to reach the minimum amplitude of the rotor flux density fundamental harmonics is 7200 mm^3, which is 18.4% lower than the reference machine. The THD of the rotor air gap flux density is 27.34%. To minimized the THD, the rotor surface is modified with the method introduced in [12]. To compensate the flux density reduction caused by the taken measures, the permanent magnet width b_{PM} is increased. In Table VI, the fundamental harmonics of the rotor flux density and the THD of the rotor with increased magnet width are

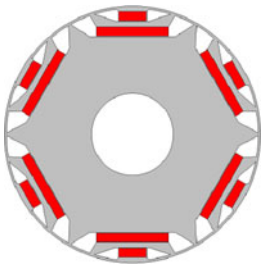

Fig. 5. Geometry of the designed IPMSM rotor.

TABLE VII
ROTOR PARAMETERS OF THE DESIGNED 2-LAYERED IPMSM

$h_{\mathrm{PM},1}, h_{\mathrm{PM},2}$	mm	2
$b_{\mathrm{PM},1}/b_{\mathrm{PM},2}$	mm	6/16
$\theta_{1,\mathrm{i}}/\theta_{1,\mathrm{o}}$	°	120/160
$\theta_{2,\mathrm{i}}/\theta_{2,\mathrm{o}}$	°	120/147.5
d_1/d_2	mm	1.5/1.25
$b_{\mathrm{barrier},1}/b_{\mathrm{barrier},2}$	mm	7.5/19.2

TABLE VIII
ROTOR AIR GAP FLUX DENSITIES

	1-Layered	VPMSM		2-Layered
	IPMSM (ref.)	Alt. 1	Alt. 2	IPMSM
Fundamental harmonic B_1 (T)	0.6	0.6	0.66	0.6
THD (%)	2.95	27.34	3.62	14.2
Magnet volume (mm^3)	8820	7200		7920

listed. It is shown that the THD of the rotor flux density is not reduced significantly after $\delta_q/\delta_d = 2.25$. For this reason, the rotor with $\delta_q/\delta_d = 2.25$ is chosen as the second alternative VPMSM (VPMSM 2). The rotor has a magnet volume of $7920\,\mathrm{mm}^3$, which is 10.20% lower than the reference machine.

In Fig. 5, the chosen design of the 2-layered IPMSM rotor is shown. The geometry parameter of the rotor are listed in Table VII. The amplitude of the fundamental air gap flux density of the rotor is 0.6 T with a THD of 14.2%. The rotor has a similar magnet volume to the VPMSM 2.

In Table VIII, the flux densities fundamental harmonic amplitude and the THD of the reference and the alternative rotors are listed. It is shown that the amplitude of the rotor flux density fundamental harmonic can be reached with lower amount of permanent magnet material. However, the reference rotor, whose rotor modification is the combination of the method described in [3] and [4], has a lower THD than the alternative rotors.

In Figs. 6 and 7, the normalized spatial behavior of the rotor flux densities in the air gap and its harmonics are shown. The flux density curve of the reference rotor is flat in the middle of the pole (d-axis) and follows the sinusoidal shape in the pole intersection. The flat area indicates the position of the uniform surface and the slope of the eccentric surface on the rotor, as described in [3]. The smooth transition at the pole intersection is induced by the application of the approach described in [4]. With the combination of these methods, all flux density harmonics can be minimized. The highest amplitudes of the harmonics are 1%

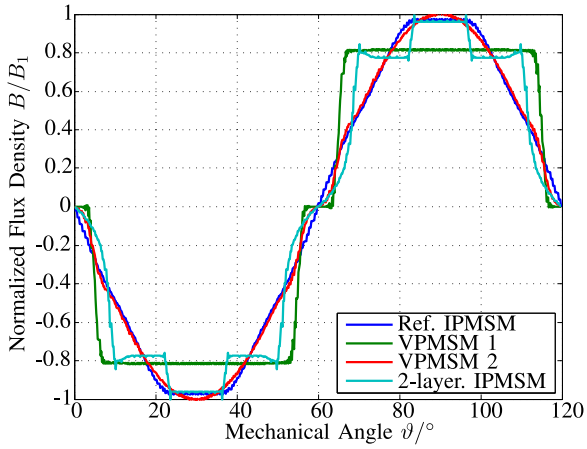

Fig. 6. Air gap flux density of the rotors normalized to the fundamental harmonics.

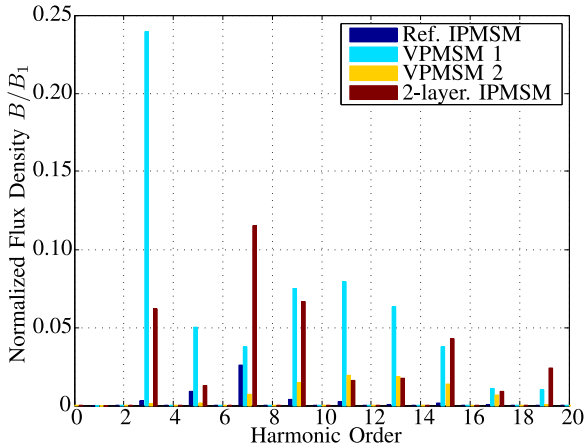

Fig. 7. Harmonics of the air gap flux density of the rotors normalized to the fundamental harmonics.

and 2.6% of the fundamental harmonic, which are the fifth and seventh harmonics of the flux density, respectively.

The effect of rotor surface modification according to Richter [12] can be seen in the flux density behavior of both VPMSMs. Without the rotor modification (VPMSM 1), the flux density has a trapezoidal shape on the d-axis with a stepped transition at the pole intersection. Due to the rotor modification (VPMSM 2), the flux density on the d-axis follows a sinusoidal function and has smoother transition on the q-axis. The distribution on the pole intersection is less sinusoidal when compared to the flux density of the reference machine. The effect of the taken measure can also be seen on the harmonics of the flux density, all of the flux density harmonics of VPMSM 2 are lower than VPMSM 1. Compared to the reference machine, VPMSM 2 has a low normalized amplitude of the third, fifth, and seventh harmonics. Starting at ninth harmonics, the normalized amplitude of the harmonics is higher than the ones of the reference machine. It can be concluded that a rotor modification near the d-axis has a dominant effect to the lower harmonics of the flux density characteristic.

The flux density characteristic of the 2-layered IPMSM is different than the 1-layered IPMSM and the VPMSM. Due to

TABLE IX
NO-LOAD SIMULATION RESULTS

	1-Layered	VPMSM		2-Layered
	IPMSM (ref.)	Alt. 1	Alt. 2	IPMSM
PM flux linkage ψ_{F} (mVs)	72.9	68.7	73.4	71.5
Inductance L_{d} (mH)	20.5	25.4	22.7	21.1
Inductance L_{q} (mH)	22.5	34.9	25.2	30.6
Saliency ratio $L_{\mathrm{q}}/L_{\mathrm{d}}$	1.1	1.37	1.11	1.45
Back EMF (phase to line) at $n = 1000\,\mathrm{min}^{-1}$ (V)	32.43	30.53	32.65	31.79
Cogging torque (mN·m)	2.5	19.8	25	82.5

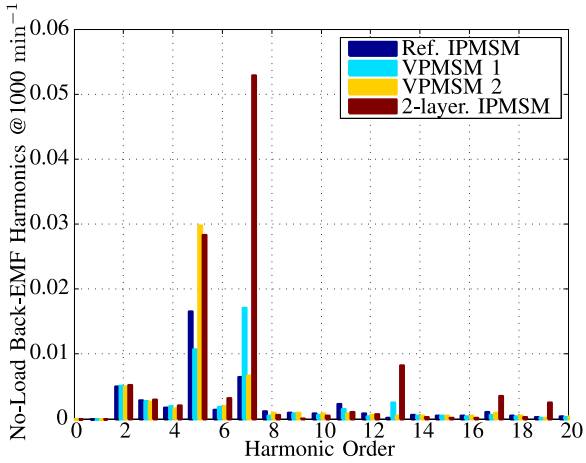

Fig. 8. Harmonics of the no-load back EMF at $n = 1000\,\mathrm{min}^{-1}$ normalized to the fundamental harmonics.

the flux barriers, the flux density has a stepped trapezoidal shape. The slopes correlates to the position of the flux barriers and the plateaus to the region on the *d*-axis and the region between the barriers (between $\theta_{1,\mathrm{o}}$ and $\theta_{2,\mathrm{i}}$). Hence, the outer angle of the second flux barrier $\theta_{2,\mathrm{o}}$ has to be wide to create a smooth transition between the pole intersection. If a small angle $\theta_{2,\mathrm{o}}$ is chosen, the transition follows the behavior of the VPMSM without surface modification. The flux density curve on the *d*-axis can be influenced through the combination of permanent magnet widths of the first and second magnet. Due to its stepped form on the *d*-axis, the third and fifth harmonics of the flux density are minimized. The normalized amplitude of its seventh harmonic is high, when compared to the other rotors.

B. No-Load Simulations

In Table IX, the simulation results of the machine in the no-load operating point are listed. Due to the similar values of the fundamental harmonic of the flux density, the permanent magnet flux linkage of the rotors is also similar to a deviation of maximum of $\pm 4\%$ to their mean value. Hence, the amplitudes of the back-EMF fundamental harmonic are also similar. The effects of the rotor modification can be analyzed through examining the relation of the back EMF and inductance in the *d*- and *q*-axis with the flux density curves and their harmonics.

In Fig. 8, the normalized back-EMF harmonics of each machine are shown. The dominant back EMF of the reference machines are the fifth and seventh harmonics, whose amplitudes are 1.65% and 0.65% of the fundamental harmonic, respectively. These are related to the dominant harmonic orders of the rotor flux density. Due to larger air gap in the *q*-axis, the inductance L_{q} is reduced and the reluctance of the machine is low when compared to a rotor without surface modification. The cogging torque of the reference machine is particularly low at 2.5 mN·m.

Due to the rotor surface alteration, the back-EMF harmonics of VPMSM 2 are generally lower than VPMSM 1. An exception occurs in the fifth harmonics, which is caused by the higher amplitude of the VPMSM 2 rotor flux density on the *d*-axis. The values of the inductance L_{d} and L_{q} are reduced due to the form of the air gap. The effect is greater on the *q*-axis, which reduces the reluctance of VPMSM 2. The cogging torque of VPMSM 2 is slightly higher than VPMSM 1, which is caused by its higher fundamental flux density and its form on the *d*-axis.

The dominant back-EMF harmonic of the 2-layered IPMSM is the seventh harmonic, which is correlated to the harmonics of the rotor flux density. The amplitude of the higher back-EMF harmonics of the 2-layered IPMSM, particularly 13th, 17th, and 19th, is also higher than the other rotors. Hence, the cogging torque of this machine is also high with 82.5 mN·m. Due to its round surface, the 2-layered IPMSM has a similar reluctance behavior to VPMSM 1.

TABLE X
OPERATING POINTS OF THE ALTERNATIVE MACHINES

	OP 1			OP 2		
Speed (r/min)	610			19520		
Torque (N · m)	1.31			0.26		
Output power (W)	83.68			531.47		
	VPMSM		2L-IPMSM	VPMSM		2L-IPMSM
Air gap ratio δ_q/δ_d	1	2.25	1	1	2.25	1
Copper losses (W)	40.63	38.87	38.88	37.89	52.97	66.55
Iron losses (W)	3.42	3.20	3.12	41.61	33.66	48.93
Efficiency (%)	65.00	66.01	66.05	81.77	80.88	77.48
Torque ripple (N · m)	0.05	0.04	0.11	0.05	0.02	0.09
Radial Force Density Orders (Temporal, Spatial) ($\mathrm{kN/m^2}$)						
(6, −3)	26.21	20.82	16.18	8.40	3.98	3.00
(6, 6)	42.19	37.14	32.57	7.82	6.26	11.71
(12, −6)	0.68	0.79	0.32	1.17	0.65	0.02
(12, 3)	6.53	2.87	0.69	3.34	1.00	0.52
(18, 0)	0.87	0.48	0.58	0.23	0.06	0.24
Magnet volume ($\mathrm{mm^3}$)	7200	7920	7920	7200	7920	7920

C. Machine Operating Points

In Table X, the simulation results of the alternative machines in both operating points OP 1 and OP 2 are listed. It should be noted that the stator winding configurations of the reference machine, VPMSM 2, and 2-layered IPMSM are identical, whereas the number of stator winding turns of the VPMSM 1 is reduced by 12% at a constant copper fill factor. The measure is taken to fulfill the requirement of minimum output power 700 W between $n = 5000 - 20\,000\,\mathrm{min}^{-1}$.

It is shown that the efficiencies of the designed machines satisfy the requirements of 62% and 74% in the base speed and field weakening operating point, respectively. The difference on the copper losses lies on the fundamental harmonic of the rotor flux densities and the saliency of the machines. The VPMSM 2 has a higher fundamental harmonic, but lower saliency than the ones of VPMSM 1 and the 2-layered IPMSM. The difference on the iron losses lies on the amplitudes of the fundamental and the higher harmonics of the rotor flux densities.

In OP 1, VPMSM 2 requires the lowest current density to reach the required torque, regardless its low saliency. This is caused by the amplitude of the rotor flux density fundamental harmonic, which is 10% higher than the other rotors. The fundamental harmonic of the VPMSM 1 and the 2-layered IPMSM is similar. The higher copper losses of VPMSM 1 are caused by the low saliency, when compared with the saliency of the 2-layered IPMSM. The iron losses of VPMSM 1 are higher than the ones of VPMSM 2 and the 2-layered IPMSM. This is caused by its high THD of the rotor flux density. The high torque ripple of the 2-layered IPMSM is caused by the high fifth and seventh harmonics of the rotor flux density, which is in total 12.8% of the fundamental harmonic. The radial force excitations, which are correlated to the acoustic radiation, are not relevant in this operating point.

In OP 2, the current density to reach the required torque depends on the field weakening behavior of the machines. Due to the arrangement of the magnets, the 2-layered IPMSM requires a high field weakening current to weaken the permanent magnet flux when compared to the VPMSM. The second permanent magnet of the 2-layered IPMSM induces the first trapezoidal curve of the flux density, which has more influence on the amplitude of the fundamental harmonic. However, the first permanent magnet has to be weakened prior to the second permanent magnet. In case of VPMSM, both magnets have the same position and can be weakened simultaneously. Because of the higher amplitude of the fundamental harmonics, VPMSM 2 requires higher field weakening current than VPMSM 1. The iron losses are dependent on the amplitude of the flux density harmonics. However, the iron losses of the 2-layered IPMSM are higher than VPMSM 1, which is generated by high flux density induced by the flux weakening current. The reason of the high torque ripple of the 2-layered IPMSM is similar to OP 1, which is the high fifth and seventh harmonics of the rotor flux density. Due to the lower THD, the radial force densities of VPMSM 2 are lower than the ones of VPMSM 1. Although the THD is low, these force densities are slightly higher than the ones of the 2-layered IPMSM. To analyze this effect, a space vector convolution according to van der Giet *et al.* [19] has to be performed. The origin of the flux density that generates these force excitations can thereby be determined.

D. Whole Operating Area

The efficiency differences of the designed machines and the reference machine $\Delta\eta = \eta_{\mathrm{alt.}} - \eta_{\mathrm{ref.}}$ for the whole operating area are presented in Fig. 9. The reference and designed machines have similar mechanical construction. Thus, the difference of the efficiencies is mainly caused by the copper and iron losses.

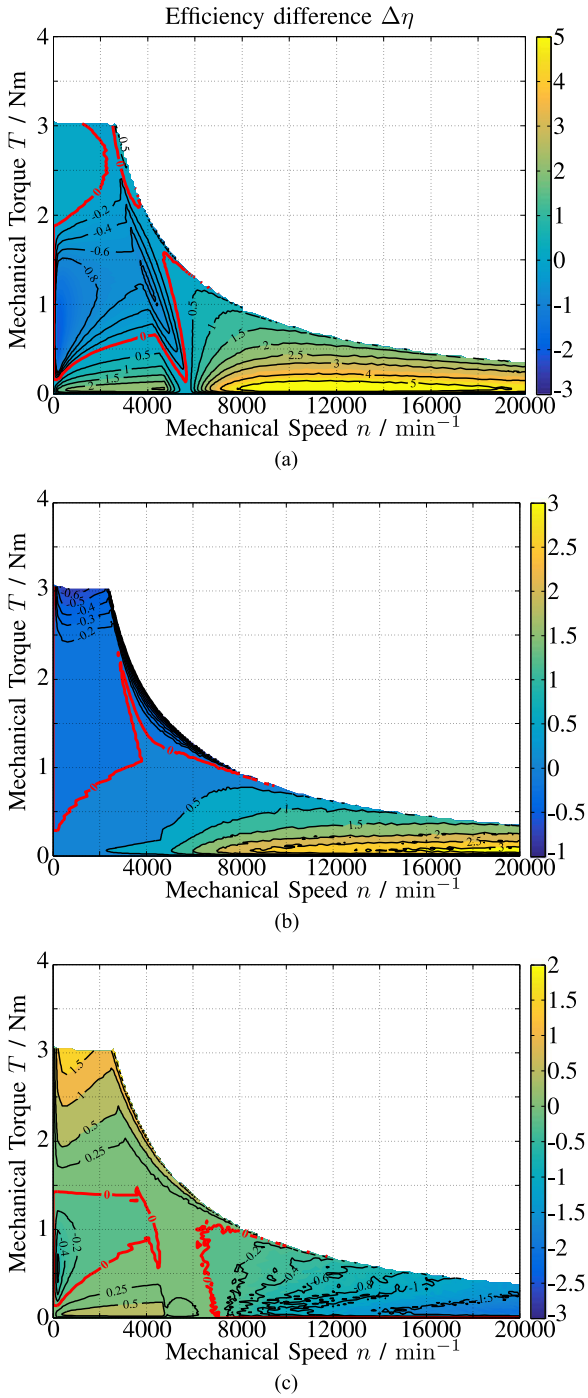

Fig. 9. Difference of the efficiencies $\Delta\eta = \eta_{\mathrm{alt.}} - \eta_{\mathrm{ref.}}$ in percentage point. (a) VPMSM 1, (b) VPMSM 2, and (c) 2-layered IPMSM.

In the base speed area, the 2-layered IPMSM has the most promising characteristics, when compared to the reference and the other designed machines. The main advantage of the 2-layered IPMSM is the combination of high permanent magnet flux linkage and high saliency ratio. It requires low currents to reach the defined torques and the copper losses are hereby lower than the other machines. At full load, the efficiencies

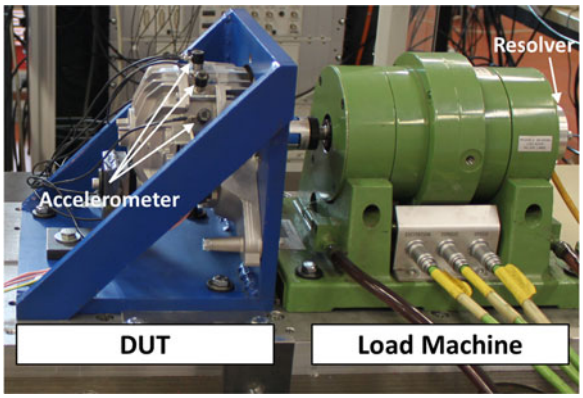

Fig. 10. Test bench setup.

of 2-layered IPMSM are about 1.5% higher than the reference machine. Due to the similar permanent magnet flux linkage and saliency ratio, VPMSM 2 has also similar characteristics to the reference machine. In case of VPMSM 1, the machine not only has a higher saliency ratio, but also has a lower permanent magnet flux linkage than the reference machine. For this reason, VPMSM 1 has mainly advantages in low torque area, in which the reluctance torque has more significant role.

In the field weakening range, both VPMSMs show advantages to the reference machine. The efficiencies of VPMSM 1 and VPMSM 2 in the field weakening ranges are up to 5% and 3% higher than the reference machine, respectively. This can be traced back to the low field weakening currents of the VPMSMs and, thus, low induced copper losses. Due to the additional permanent magnet material, the required field weakening currents of VPMSM 2 and also the copper losses are slightly higher than VPMSM 1. However, the iron losses are low due to the low harmonic amplitudes of the rotor flux density. The efficiencies of the 2-layered IPMSM in the field weakening area are generally lower than the reference machine. This lies on the high required field weakening current and the induced iron losses of the machine.

V. Measurement Results

In this section, the measurement results of the reference and the designed machines are presented. Additional to the existing reference machine, one stator with the winding configuration of the reference machine and two rotor geometries (VPMSM 1 and VPMSM 2) are constructed for this purpose.

A. Test Bench Setup

The measurement setup is depicted in Fig. 10. The device under test (DUT) is directly coupled with a brake to minimize the axial length of the setup. A speed control is applied to the DUT, while the brake delivers a braking torque. The control is implemented in a rapid prototyping system. The motor currents as well as torque, speed, and angular position are measured and processed in the controller, which generates the duty cycles of a three-phase voltage controlled inverter. For the no-load operating point, another load machine is used to drive the DUT and the cogging torques are measured with a torque transducer.

TABLE XI
No-Load Measurement Results

	Ref. IPMSM	VPMSM 1	VPMSM 2
PM flux linkage ψ_{F} (mVs)	74.1	64.6	68.9
Inductance L_{d} (mH)	18.4	22.7	21.1
Inductance L_{q} (mH)	22.3	31.6	25.1
Saliency ratio $L_{\mathrm{q}}/L_{\mathrm{d}}$	1.21	1.39	1.19
Back EMF (phase to line) at $n = 1000\,\mathrm{min}^{-1}$ (V)	32.9	28.7	30.6
Cogging torque (mN·m)	2.2	14.9	17.5

TABLE XII
Measurement Results at Machine Operating Points

	OP 1			OP 2		
	Ref.	VPMSM		Ref.	VPMSM	
	IPMSM	Alt. 1	Alt. 2	IPMSM	Alt. 1	Alt. 2
Efficiency (%)	71.0	66.5	69.8	73.0	81.3	80.4
Torque ripple ($\mathrm{N}\cdot\mathrm{m}$)	0.03	0.03	0.03	< 0.01	< 0.01	< 0.01
Maximum Surface Velocity Orders (Temporal, Spatial) ($\mathrm{mm/s}$)						
(6, −3)		–		1.12	0.80	0.64
(12, 3)		–		0.18	0.37	0.13

To measure the stator vibration, ten uniaxial accelerometers are magnetically mounted on the surface of the stator. A stator deformation up to spatial mode $r = 5$ can hereby be measured.

B. Operating Area

The measurement results in the no-load operating point are presented in Table XI. The measured machine parameters and back EMF show good agreements with the simulation results, with a maximum deviation of 10% in inductance. The measured cogging torques are up to 30% lower than the simulated ones. This is caused by the low permanent magnet flux linkage and high reluctivity of the built machines, when compared to the simulated machines.

The measurement results in OP 1 and OP 2 are presented in Table XII. The measured efficiencies show good agreements with the simulated ones. The deviations can be traced back to the temperatures of the machines, which are not logged during the measurements. The vibration measurements are only performed at acoustic relevant operating point, which is OP 2. According to DIN ISO 5348, vibration up to 5 kHz can be measured using magnetic mounted acceloremeters. Thus, the order (18, 0) with a frequency of 5856 Hz is not analyzed. The relevant vibration modes can be identified through visualization of the accelerometers position, which is illustrated in Fig. 11 for $f = 1952\,\mathrm{Hz}$. It can be seen that the third mode is dominant in this frequency. The surface velocity rotates in the opposite direction to the rotor's rotation, which corresponds to the orders (6, −3). The dominant mode for $f = 3904\,\mathrm{Hz}$ is also determined by this method. In this case, the dominant order is (12, 3) and the rotation direction of the surface velocity is the same with the rotor's rotation direction. For these reasons, the evaluations of the vibration measurements are only performed for the dominant orders (6, −3) and (12, 3). The machines comparative

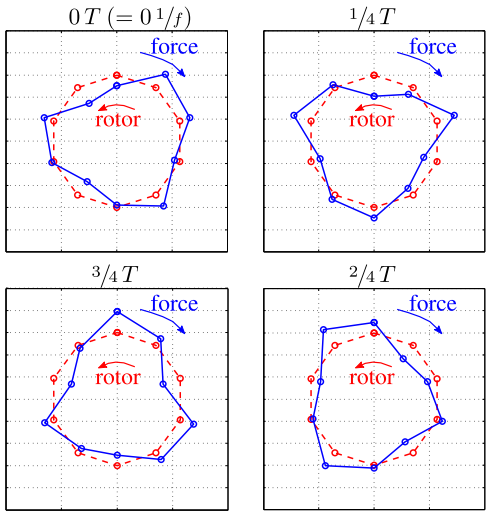

Fig. 11. Surface velocities rotation of the reference machine at OP 2 and $f = 1952\,\mathrm{Hz}$ (measured).

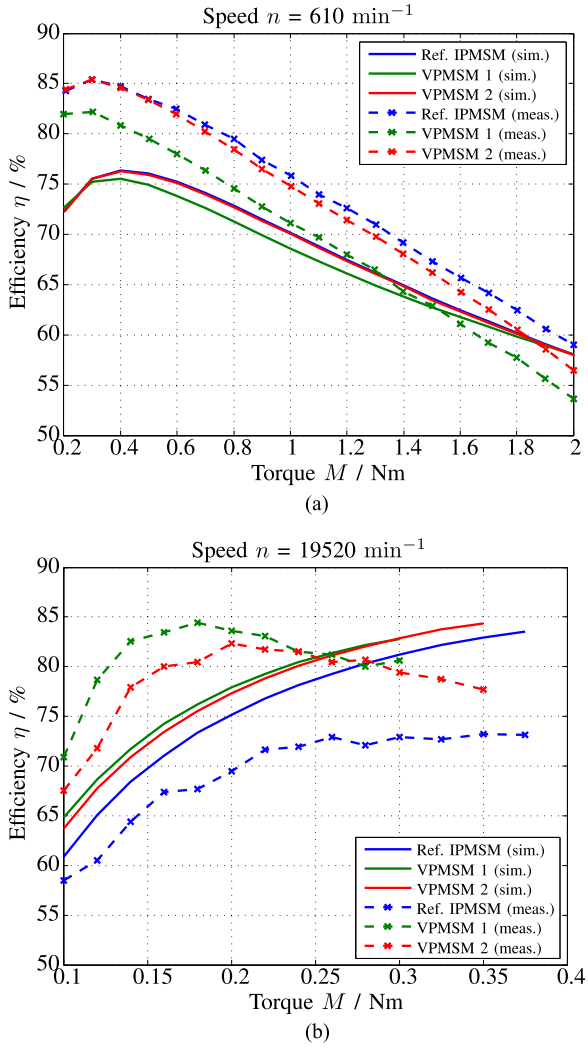

Fig. 12. Comparison of simulation and measurement results. (a) Efficiencies at $n = 610\,\mathrm{min}^{-1}$. (b) Efficiencies at $n = 19520\,\mathrm{min}^{-1}$.

behaviors of the simulated force densities and measured surface velocities show good agreements. The deviations in order $(6, -3)$ of the reference machine and VPMSM 1 can be caused by manufacturing tolerances.

The measurement results in other operating areas at $n_1 = 610\,\mathrm{min}^{-1}$ and $n_2 = 19520\,\mathrm{min}^{-1}$ are illustrated in Fig. 12. In general, the deviations are caused by the temperature differences between simulations and measurements. In addition, the used converter has a switching frequency of 10 kHz and cannot produce a sinusoidal current at $f_{\mathrm{el.}} = 976\,\mathrm{Hz}$ ($n_2 = 19520\,\mathrm{min}^{-1}$) to feed the machine. This causes increase in the iron losses and decrease in the efficiencies.

VI. Conclusion

Three PMSM are designed as alternatives to a reference machine. The machines have lower magnet volume than the reference machine and satisfy the requirements concerning the efficiencies in relevant operating points OP 1 and OP 2. The behavior of the machines in OP 1, except the torque ripple of the 2-layered IPMSM, are similar to each other. In OP 2, VPMSM 2 shows a good balance between high efficiency, low torque ripple, and radial force excitation.

A VPMSM without rotor modification has a good agreement between the synchronous and reluctance torque. The rotor requires the lowest magnet volume to reach the minimum amplitude of the rotor flux density fundamental harmonics and has a good $L_{\mathrm{q}}/L_{\mathrm{d}}$ ratio. Due to the high THD of the rotor flux density, the rotor has a disadvantage regarding its parasitic effects. The torque ripple, radial force excitations, and the iron losses are particularly high. To subdue this effect, the rotor surface is modified, which leads to the decrease in the rotor flux density harmonic amplitudes and the reluctance characteristic. As a compensation, the amount of the used permanent magnet material has to be increased. In this case, with 10% increase on magnet material, a machine with similar efficiencies but lower torque ripple and radial force excitations is designed. The increase in the copper losses in the field weakening range due to lower saliency evens the decrease in the iron losses. A 2-layered IPMSM exhibit a high reluctance torque, but low synchronous torque when compared to a VPMSM. The advantage of a 2-layered IPMSM over VPMSM is the possibility to manipulate the form of the rotor flux density without rotor surface modification and the reluctance torque is thereby preserved. However, 2-layered IPMSM has a disadvantage in field weakening range. The permanent magnet near the air gap has to be weakened prior to the second permanent magnet, which increase the required flux weakening current and the iron losses. The torque ripple is also high, when compared to a VPMSM with surface modification. The radial force excitations of both machines are similar to each other.

Concerning the machine characteristics in both operating points, the VPMSM with surface modification is chosen as the most suitable alternative to the reference machine. The prototypes of the designed VPMSMs as well as the reference machine are built. The measurement results show good agreements with the simulation results.

REFERENCES

[1] B. E. Donald, D. W. Novotny, and T. A. Lipo, "Field weakening in buried permanent magnets ac motor drives," *IEEE Trans. Ind. Appl.*, vol. 21, no. 2, pp. 398–407, Mar./Apr. 1987.

[2] W. Soong nad T. J. E. Miller, "Field weakening performance of brushless synchronous ac motor drives," *IEEE Proc.-Elect. Power Appl.*, vol. 141, no. 6, pp. 331–340, Nov. 1994.

[3] K.-Y. Hwang, S.-B. Rhee, B.-Y. Yang, and B.-I. Kwon, "Rotor pole design in spoke-type brushless dc motor by response surface method," *IEEE Trans. Magn.*, vol. 43, no. 4, pp. 1833–1836, Apr. 2007.

[4] K.-W. Jeon, T.-Y. Lee, Y.-J. Kim, and S.-Y. Jung, "Numerical shape design characteristics of torque ripple reduction for interior permanent magnet synchronous motor," in *Proc. Int. Conf. Comput. Electromagn.*, London, U.K., 2014, pp. 1–2.

[5] F. Henrotte, M. Felden, M. van der Giet, and K. Hameyer, "Electromagnetic force computation with the eggshell method," in *Proc. 14th Int. Symp. Numer. Field Calculation Elect. Eng.*, Graz, Austria, 2010, 6 pages.

[6] F. Henrotte, G. Deliege, and K. Hameyer, "The eggshell approach for the computation of electromagnetic forces in 2D and 3D," *COMPEL—Int. J. Comput. Math. Elect. Electron. Eng.*, vol. 23, no. 4, pp. 996–1005, 2004.

[7] S. A. Gelfand, *Essentials of Audiology*. New York, NY, USA: Thieme Med. Publ., 2009.

[8] D. Eggers, S. Steentjes, and K. Hameyer, "Advanced iron-loss estimation for nonlinear material behavior," *IEEE Trans. Magn.*, vol. 48, no. 11, pp. 3021–3024, Nov. 2012.

[9] S. Steentjes, D. Eggers, M. Lessmann, and K. Hameyer, "Iron-loss model for the FE-simulation of electrical machines," in *Proc. INDUCTICA Tech. Conf.,/Coil Winding, Insul. Elect. Manuf. Int. Confe. Exhib.*, Berlin, Germany, 2012, pp. 239–246.

[10] R. De Doncker, D. Pulle, and A. Veltmann, *Advanced Electrical Drives: Analysis, Modeling, Control*. New York, NY, USA: Springer, 2010.

[11] A. Wang, Y. Jia, and W. L. Soong, "Comparison of five topologies for an interior permanent-magnet machine for a hybrid electric vehicle," *IEEE Trans. Magn.*, vol. 47, no. 10, pp. 3606–3609, Oct. 2011.

[12] R. Richter, *Elektrische Maschinen: Allgemeine Berechnungselemente*. Basel, Switzerland: Birkhäuser, 1951.

[13] C. Andrei *et al.*, "Improved PMSM for wind turbine applications with multiple high-speed generators," *J. Elect. Eng.*, vol. 16, no. 1, pp. 1582–1594, 2016.

[14] S. A. Evans, "Salient pole shoe shapes of interior permanent magnet synchronous machines," in *Proc. 19 Int. Conf. Elect. Mach.*, Rome, Italy, 2010, pp. 1–6.

[15] T. Finken, "Fahrzyklusgerechte Auslegung von permanentmagneterregten Synchronmaschinen für Hybrid- und Elektrofahrzeugen," Ph.D. dissertation, Faculty Elect. Eng. Inf. Technol., RWTH Aachen University, Aachen, Germany, 2011.

[16] L. Fang, J.-W. Jung, J.-P. Hong, and J.-H. Lee, "Study on high-efficiency performance in interior permanent-magnet synchronous motor with double-layer PM design," *IEEE Trans. Magn.*, vol. 44, no. 11, pp. 4393–4396, Nov. 2008.

[17] S. Rick, A. K. Putri, D. Franck, and K. Hameyer, "Permanent magnet synchronous reluctance machine—Design guidelines to improve the acoustic behavior," in *Proc. 21st Int. Conf. Elect. Mach.*, Berlin, Germany, 2014, pp. 1383–1389.

[18] A. K. Putri, M. Hombitzer, D. Franck, and K. Hameyer, "Cost-oriented design of high speed low power interior permanent magnet synchronous machines," in *Proc. 22nd Int. Conf. Elect. Mach.*, Lausanne, Switzerland, 2016, pp. 1448–1454.

[19] M. van der Giet, R. Rothe, M. H. Gracia, and K. Hameyer, "Analysis of noise exciting magnetic force waves by means of numerical simulation and a space vector definition," in *Proc. 18th Int. Conf. Elect. Mach.*, Vilamoura, Portugal, 2008, pp. 1–6.

Aryanti Kusuma Putri received the M.Sc. degree in electrical engineering from RWTH Aachen University, Aachen, Germany, in April 2013.

She has been a Research Associate in the Institute of Electrical Machines, RWTH Aachen University, since June 2013. Her research interests include contactless power transmission, parasitic effects in electrical machines, and simulation and design of electrical machines.

Marco Hombitzer received the Dipl.-Ing. degree in electrical engineering from RWTH Aachen University, Aachen, Germany, in 2010.

Since 2010, he has been a Researcher in the Institute of Electrical Machines, RWTH Aachen University. His research fields include the simulation, design, and performance improvement of electrical machines.

David Franck received the Dipl.-Ing. degree in electrical engineering from RWTH Aachen University, Aachen, Germany, in March 2008.

He was a Research Associate in the Institute of Electrical Machines, RWTH Aachen University, where he has been a Chief Engineer since 2011. His main field of research is the acoustic behavior of the electrical machines.

Kay Hameyer (M'96–SM'99) received the M.Sc. degree in electrical engineering from the University of Hannover, Hannover, Germany, and the Ph.D. degree from the Berlin University of Technology, Berlin, Germany.

He was with the Robert Bosch GmbH, Stuttgart, Germany, as a Design Engineer for permanent magnet servo motors and vehicle board net components. Until 2004, he was a Full Professor for numerical field computations and electrical machines with the KU Leuven, Belgium. Since 2004, he has been a Full Professor and the Director of the Institute of Electrical Machines, RWTH Aachen University, Aachen, Germany. In 2006, he was the Vice Dean of the Faculty of Electrical Engineering and Information Technology, and from 2007 to 2009, he was the Dean of the Faculty of Electrical Engineering and Information Technology. He is the author of more than 250 journal publications, more than 500 international conference publications, and author of 4 books. His research interests include numerical field computation and optimization, the design and controls of electrical machines, in particular permanent magnet excited machines, induction machines, and the design employing the methodology of virtual reality. His work is concerned with the magnetic levitation for drive systems, magnetically excited audible noise in electrical machines, and the characterization of ferro-magnetic materials.

Dr. Hameyer is a member of VDE and a fellow of the IET.